TUNING MOLECULAR SEPARATION TO IMPROVE DETECTION SENSITIVITY IN SOLUTION-BASED ASSAYS

By

ZHAOLIN XUE

A thesis submitted to the

School of Graduate Studies

Rutgers, The State University of New Jersey

In partial fulfillment of the requirements

For the degree of

Master of Science

Graduate Program in Materials Science and Engineering

Written under the direction of

Laura Fabris

And approved by

_____

_____

_____

New Brunswick, New Jersey

May 2020

ABSTRACT OF THE THESIS

Tuning Molecular Separation to Improve Detection Sensitivity in Solution-based Assays

by ZHAOLIN XUE

Thesis Director:

Laura Fabris

Metal nanoparticles have unique physical and optical properties stemming from their nanoscale dimensions, inducing strong localized surface plasmon resonance (LSPR), which lead them to find extensive applications in chemi-sensors and biosensors. By concentrating the incident electromagnetic (EM) field near the nanostructure, LSPR modes can enhance the local scattered EM field and affect optical processes such as Raman scattering and fluorescence, giving rise to the so-called surface-enhanced Raman scattering (SERS) and plasmon-enhanced fluorescence (PEF). Because they both depend on the distance between the reporting molecules and the nanoparticles but at different regimes, SERS and PEF become dominant separately and can be thus leveraged to design orthogonal transduction mechanisms.

In this thesis, the detection sensitivity in solution-based assays enabled by portable SERS and molecular beacon-based fluorescence are improved by keeping the molecules close to or properly away from the surface of the nanoparticles.

For the first part, opioid drug molecules are attracted to the surface of silver nanoparticles and trapped in the “hot spots” to achieve SERS enhancement through aggregation induced by salt addition. Salting optimization and aggregation dynamics analysis are carried out for improving drug detection. NaBr solution is chosen as the aggregation inducing salt at the

optimal concentration of 1 M with 3 minutes time window for detection. The improved assay supports a LOD of ~5 ng/mL for fentanyl spiked in urine controls and a LOD of ~0.1 % (10 ng in 10 μg total) mass percent for fentanyl in laced recreational drugs such as heroin or THC, which surpasses the results achieved in comparable previous reports.

For the second part, fluorophores in molecular beacons (MBs) are pushed away from the surface of gold nanoparticles via hybridization of the beacons with nucleic-acid strand targets, but still kept at a well-known distance which depends on the length of the MBs, thus facilitating PEF and generating enhanced fluorescence signals. A single strand DNA with ten thymine groups (T_{10}) is also implemented as a spacer to assist the stretching process of MBs via reduction of steric hindrance. Functionalization of MBs on the surface of gold nanoparticles is performed along with the optimization of reaction conditions. Based on the fluorescence enhancement, the proper molar ratio of MBs/ T_{10}-to-gold nanoparticles is 1000/1 for a relatively strong and stable signals enhancement. And the ratio of MBs-to-T_{10} within the range of 3~5 has relatively less influence on the result. Calibration curves for the MBs gold nanoparticles sensor are generated under different concentrations of nucleic-acid strand targets, indicating a LOD of ~10 nM for room temperature detection and a LOD of ~20 nM at 37.5 ℃.

Table of Contents

List of Illustrations

Chapter 1 Introduction

1.1 Background

In the last few decades, the design and synthesis of nanomaterials with dimensions ranging between 1 and 100 nm have grown rapidly, leading to the development of innovative biosensing systems and the improvement of bioanalytical assays.[1] Nowadays, well-developed synthetic protocols make it relatively easy to produce high-quality nanoparticles of various morphology, such as nanospheres, nanostars, and nanorods, among others.[2, 3] These nanoparticles play an essential role in the design of biosensors due to their large surface-to-volume ratio, and significant size and shape dependent properties, compared to micro-scale or bulk materials. Binding events involving biomolecules can be detected monitoring the optical and electronic response of nanoparticle-based biosensors. Particularly relevant transduction mechanisms in this respect are surface enhanced Raman scattering and fluorescence, which respond to recognition events through variations in peak position and peak intensity for specific analyte or reporter molecules.[4, 5]

1.2 Surface-enhanced Raman scattering (SERS) and plasmon-enhanced fluorescence (PEF)

Raman scattering occurs upon inelastic collision of photons with molecules, in which the excitation photons couple to the characteristic molecular vibration of the molecule, re-emitting the scattered photons at different frequency.[6, 7] Because different molecular vibrations generate different Raman scattering signals, this technique provides a unique vibrational “fingerprint” for the target analyte. The scattering intensity of a Raman signal depends on the excitation intensity and the probability of vibrational excitation, which can be determined in terms of optical cross section. The optical cross section is related to the polarizability derivative of the molecular vibration, described as the transverse area on the molecule that the incident photons hit converting the impinging photons into scattered Raman

photons. In general, the Raman scattering process has low cross sections (ca. 10^{-11} to 10^{-15} nm^2 per molecule) which are insufficient for sensing applications when the target analytes are present at concentrations lower than 1 mM.[8]

A surface plasmon is the collective oscillation of conduction electrons in metallic nanostructure at the interface with a dielectric medium in response to an impinging electromagnetic radiation.[9] Both the size, shape and composition of metallic nanostructure, as well as the dielectric properties of the surrounding medium have a strong impact on the intensity and the position of the plasmon modes.[10-13] There are two types of surface plasmons, the localized surface plasmons (LSPs) and the propagating surface plasmon polaritons (SPPs). LSPs originate when the size of the metallic nanostructure is smaller than the wavelength of the incident light, and the collective oscillation is confined by coulombic restoring force to form an oscillating dipole with specific resonant frequency, also known as the localized surface plasmon resonance (LSPR). LSPs can locally increase the electromagnetic (EM) field by concentrating the incident EM field around the nanostructure, with effects on optical processes such as fluorescence and Raman scattering that lead to plasmon-enhanced fluorescence (PEF) and SERS.[14]

After almost 45 years since the discovery of SERS, researchers have reached a general consensus on it fundamental mechanism; both electromagnetic (EM) enhancement and chemical (CHEM) enhancement contribute to the overall SERS enhancement, with the former however dominating the effect.[15-17] The EM enhancement stems from the plasmonic excitation, and the resulting amplified local EM field around the metal nanoparticles. The CHEM enhancement, on the other hand, originates from charge transfer processes between the metal nanoparticles and the adsorbed molecules. The Raman scattering can be enhanced through the EM and the CHEM mechanisms up to 10-12 orders of magnitude, an increase that is quantified by the so-called enhancement factor (EF). The most significant EFs occur when the molecules are in the immediate vicinity of corrugated metal surfaces such as gold or silver nanoparticles, due to the high local EM field from the coupling of surface plasmons. The EM

enhancement normally has larger contributions to SERS, yielding the EFs around 10^4 to 10^8, compared to the CHEM enhancement with the EFs from 10 to 100.[18] Primarily, in suitable resonant metal nanostructure, local plasmon fields can dramatically amplify the initial absorption process through resonances between the optical field and the surface plasmons, leading to a large optical field enhancement. The effective SERS cross section are comparable to fluorescence cross sections, enabling Raman measurements at the single molecule level.

Plasmon-enhanced fluorescence (PEF) can be also referred to as metal-enhanced fluorescence (MEF); similarly, the resulting spectroscopic techniques can be defined both as surface plasmon-enhanced fluorescence spectroscopy (SPFS) or surface-enhanced fluorescence spectroscopy (SEFS). The mechanisms of PEF can be understood when the plasmon and the fluorophore are described as dipole. As is well known, fluorescence originates when a molecule absorbs light at specific wavelength and subsequently emits photons at longer wavelength due to radiative relaxation from an excited electronic state. The excited singlet electronic state, from which fluorescence originates, can be explained following a radiative dipole model, in which excitation, relaxation, and emission are induced by incident light.[19]

The interaction between a plasmonic dipole and a radiative dipole induces energy transfer between the fluorophore and the plasmon, with efficiency that depends on the separation distance between the two. If the distance between plasmon and fluorophore is within 1 to 10 nm, Förster resonance energy transfer (FRET) will occur, which means that the non-radiative local field of one dipole can excite the other one, transferring energy from plasmon to fluorophore or vice versa. The separation distance R and the spectral distance R_0 are used to describe the efficiency of energy transfer in FRET.[20]

$$\mathrm{Eff_{FRET}} = \frac{1}{1+\left(\frac{R}{R_0}\right)^6} \tag{1}$$

The efficiency is correlated to $1/R^6$ because there is a $1/R^3$ near field dependence in each dipole. The factor R_0 (i.e. the separation at which the FRET efficiency is 50%) depends on the degree of spectral overlap between the emission of the donor and the absorption of the

acceptor. When a plasmon is located at a distance R from a fluorophore that is shorter than R_0 ($R < R_0$), the efficiency of FRET will be very high, approaching 100%, on account of the amplified local field and large absorption cross section originated from the LSPR. In plasmon-fluorophore FRET, R_0 is usually at around 3 to 8 nm.

Secondly, the Purcell effect, i.e. the effect of the surrounding media on the emission properties of an emitter, also plays a part in plasmon-fluorophore interactions.[21] A resonant cavity can modify the local density of optical states (LDOS) based on the intensity of the local electric field increasing the LDOS peak at the resonance wavelength. On the one hand, a radiative dipole in the cavity can emit into this mode at a higher rate than it emits in air, as if coupling into an antenna. Then, the transferred energy will be re-radiated by the cavity, leading to an overall enhancement of the dipole emission. On the other hand, if the dipole in the resonant cavity has an off-resonance radiation, the transferred energy will be absorbed, resulting in a quenching of emission intensity. Both plasmon and fluorophore can act like the resonant cavity for each other. But since the local electric field of fluorescence is usually on the level of free space and cannot lead to an increased LODS, the resulting Purcell effect from a "fluorescent cavity" is negligible.[22]

The spectral overlap and separation distance between the plasmon and the fluorophore are two crucial factors. The magnitude of the FRET and the Purcell effects can be altered based on these factors, causing an enhancement or quenching of the fluorophore emission. The LDOS has a $1/R^3$ near field, presenting the Purcell effect outside the approximately 10 nm range of $1/R^6$ non-radiative transfer in the FRET.[22-24] When the plasmon is overlapped with the absorption of fluorophore, the enhancement of the fluorophore's excitation rate will occur; this result stems from the FRET process, where the energy transfers from the plasmon to the fluorophore. The Purcell effect of plasmon cavity tends instead to absorb energy from the fluorophore due to the off-resonance emission of the fluorophore in the cavity, while the Purcell effect of fluorophore cavity is negligible, as mentioned. When the plasmon spectrally overlaps with the fluorophore emission, an enhancement or quenching of fluorophore

emission intensity will occur based on the separation distance. The fluorophore emission will be quenched due to FRET energy transfer from fluorophore to plasmon when the separation distance is around few nanometers. The plasmon will also be excited to higher order modes by the near field dipole, impeding the far field re-radiation of plasmon, resulting in an overall quenching of the emission. The fluorophore emission enhancement will be induced because of the dominance of the Purcell effect, leading to an increase of the radiative rate when the separation distance is beyond that leading to FRET. Therefore, fluorophore emission is quenched within few nanometer separation distance, and enhanced 10 to 100 times when the distance increases to 10~30 nm, then gradually decreased to its normal emission intensity when the distance approaches to around 100 nm.[19] Metal nanoparticles with a small size (＜ 15 nm) generally favor FRET due to the high absorption efficiency of light in plasmon, while larger metal nanoparticles (＞15 nm), which are better scatterers than absorbers, benefit the Purcell effect.[25, 26]

1.3 Nanoparticle-based biosensors

Generally speaking, metals with high optical reflectivity as well as negative real part and relatively small positive imaginary part of dielectric constant, such as gold, silver or copper, are ideal materials for SERS or PEF. On the contrary, transition metals like Fe, Ni and Pd that have low optical reflectivity cannot induce a sufficient SERS effect.

Although local EM field enhancement can be obtained and induce measurable SERS enhancement on the surface of single nanoparticles, an even more intensive local EM field can be achieved by a more elaborate nanoparticle construct, such as when a nanometer-sized gap between two metal particles, so called “hot spot”, can be created, which allows EFs to reach values up to 10^{12}.[27, 28] The EM field intensity at the gap strongly depends on the gap distance. A common method to bring particles closer in suspension is to add electrolytes, inducing a “salting out” effect.[29, 30] For example, in a classical preparation of gold or silver colloids, the particles’ surface is decorated with negative charges owing to the presence of

sodium citrate, which serves as both reducing agent and stabilizer. The addition of electrolytes such as sodium chloride to this citrate-coated colloidal solution will lead to a compression of the diffuse layer of the electrical double layer, lowering the value of the zeta-potential and reduce the electrostatic repulsive force. According to the Derjaguin, Landau, Verwey, and Overbeek (DLVO) theory, the interaction energy barrier will decrease when the electrostatic repulsion decreases with constant van der Waals attraction. Hence, the metallic particles are not stable, trend to aggregate, and "salt out". By taking advantage of particle aggregation and formation of "hot spots" (i.e. the intermetallic junctions between NPs), silver nanoparticles (AgNPs) can be utilized as the SERS substrate to detect different sequence of DNA/RNA mononucleotides at ppm level in the presence of magnesium sulfate.[30]

In recent years, gold nanoparticle probes based on bioconjugated nucleic acids have caught substantial attention due to their ability to detect various targets such as nucleic acids, ions, molecule metabolites, and proteins in living cells.[31] The nucleic acids can be easily modified with fluorophore at desired positions along the strand, and designed to detect other complementary nucleic acid sequences. Moreover, the assembly of nucleic acids on the nanoparticle surface results in what have been defined as spherical nucleic acids (SNAs) which have been shown to be taken up by cells without the need for toxic transfection agents, benefiting substantially the intracellular analysis.[32] Among the variety of nucleic acids constructs that can be bound on gold nanoparticles, molecular beacons (MBs) offer many important advantages, including impediment to nuclease degradation and easy direct entrance into living cells.[33] As shown in **Figure 1**, a gold nanoparticle MBs can be considered as several dye-labeled hairpin sequences which are formed by self-hybridization of the complementary flanks on the single stranded DNA, functionalized to a gold nanoparticle. In the absence of target, the hairpin is closed, anchoring the dye in close proximity to gold surface, quenching the fluorescence. When the target strands (e.g. mRNA, RNA, DNA) hybridize with the single stranded DNA probe, the hairpin opens up, separating the dye from the gold nanoparticle and turning on the fluorescence. Note that understanding and

modulating the steric hindrance on the nanoparticle as well as the energy barrier of the DNA hybridization are essential toward achieving the unfolding of the beacon. Non-reactive single stranded DNA can be added onto the gold nanoparticles surface as a spacer to reduce steric hindrance by creating enough space between MBs.[34] By carefully designing the MB sequence and calibrating the relative amounts of beacon and spacer, it is possible to achieve hairpin unfolding and straightening so that the sufficient distance between metal and fluorophore can be obtained to obtain fluorescence enhancement while still within the range of PEF effect.

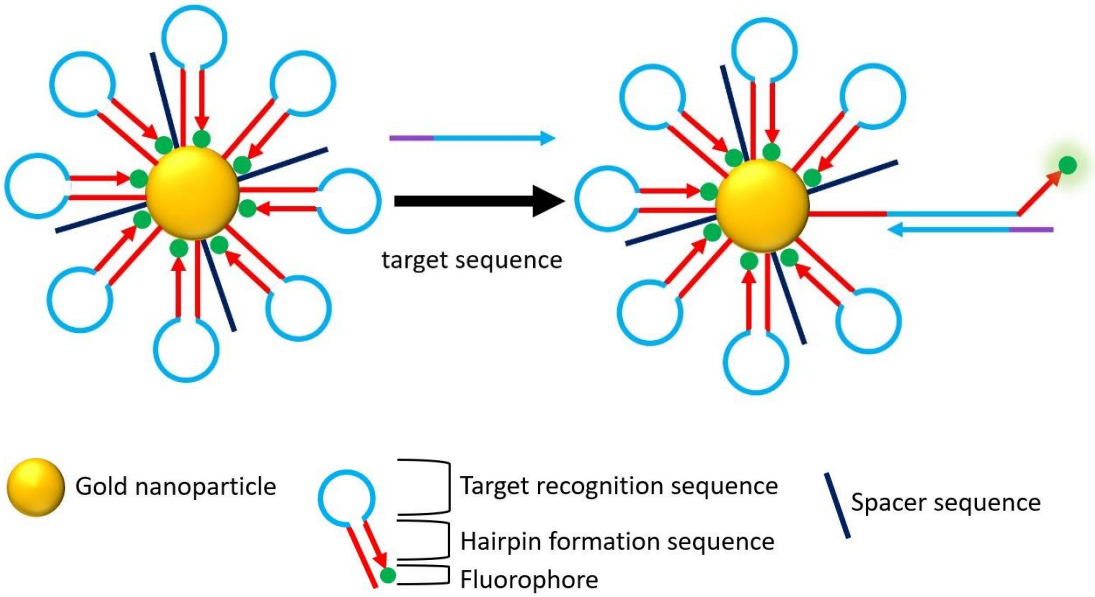

Figure 1. Sketch of gold nanoparticle molecular beacons and the fluorescence recovery process in the presence of target sequence.

1.4 Objective and overview

In summary, it has been demonstrated that SERS has a huge potential in many biomedical applications, presenting an ultrasensitive detection approach for analytes up to extremely low concentration levels and high selectivity. Nanoparticle assemblies created via the "salting out" process lead to the generation of numerous "hot spots" in which analyte molecules are captured, further enhancing the SERS signal. Moreover, gold nanoparticles MBs, have the potential to target nucleic acids in living cells and report on their presence and amount via fluorescence signaling. The gold nanoparticles MBs normally stay on a fluorescence-quenched and SERS-ON state without targets while easily switching to a fluorescence-ON and SERS-off state at the presence of targets.

This thesis will focus on two parts. In the first part, the objective is to improve limits of detection in solution-based fentanyl assay to be carried out with portable spectrometers to enable low-cost rapid identification. This method leverages silver nanoparticles aggregation to achieve not only high sensitivity but also high selectivity. Synthesis and characterization of AgNPs have been carried out along with SERS validation and salting optimization. Then the fentanyl detection in water, artificial urine, and multicomponent solution was carried out. In the second part, the goal is to improve the sensitivity of short single stranded DNA detection in vitro based on the switchable fluorescence effect of gold nanoparticles MBs. The influence of several factors during synthesis, such as the molar ratio of particles to MBs and MBs to spacer, on the performance of final particles-MBs product are explored.

Chapter 2 Improving Trace Fentanyl Detection in Portable SERS

Fentanyl, as a synthetic opioid drug that can shut down breathing in less than a minute, has induced an exponential growth of fatal overdose in the US since 2013.[35] Along with the trend of filling or adulteration in other recreational drugs such as marijuana and heroin, fentanyl abuse has already emerged as a prominent threat to public health.[36] Hence, for the purposes of drug control and tracking in the field, it is important to develop an efficient detection tool on a portable platform for rapid identification and quantification of fentanyl-laced drugs.

The emergence of SERS offers an advanced technique with high sensitivity and specificity for many applications, such as biomedical imaging, photocatalysis, and ultrasensitive detection.[37, 38] In recent years, the implementation of SERS in quantitative drug analysis via the use of highly ordered substrates or paper substrates has gained great attention;[39-42] however, these methods are restricted to either costly production, or the need for sophisticated Raman equipment, or substrate degradation and inhomogeneity.

In this work, a solution-based SERS assay carried out via a portable Raman spectrometer is developed and improved, presenting more sensitive and reliably quantitative properties than previously reported.[43-48] By turning the particles closer and optimizing the conditions for inducing aggregation, this assay allows a limit of detection (LOD) of ~5 ng/mL for fentanyl spiked in urine and ~0.05% and ~0.1% mass concentration for fentanyl laced in heroin and THC respectively.

2.1 Materials and Method

2.1.1 Materials

Silver nitrate ($AgNO_3$; ≥99.995%), trisodium citrate dihydrate ($C_6H_5O_7Na_3 \cdot 2H2O$), sodium chloride (BioXtra; ≥99.5%), sodium bromide (BioXtra; ≥99.0%), sodium iodide dihydrate ($NaI \cdot 2H_2O$; ≥99.0%), sodium sulfate (Na_2SO_4; ≥99.0%), crystal violet ($C_{25}H_{30}N_3Cl$; ≥90%),

rhodamine 6G ($C_{28}H_{31}ClN_2O_3$; ~95%), caffeine ($C_8H_{10}N_4O_2$), fentanyl solution (1.0 mg/mL in methanol, Cerilliant®), norfentanyl oxalate solution (1.0 mg/mL in methanol, Cerilliant®), Surine™ negative urine control (Cerilliant®, an odorless artificial urine with constituents that mimic human urine, pH~6.9, light yellow), (-)-trans-Δ^9-THC solution (1.0 mg/mL in methanol, Cerilliant®), heroin solution (1.0 mg/mL in acetonitrile, Cerilliant®), heroin hydrochloride solution (100 μg/mL in methanol), oxycodone solution (1.0 mg/mL in methanol, Cerilliant®), morphine solution (1.0 mg/mL in methanol, Cerilliant®) were all purchased from Sigma Aldrich. All these chemicals were used without further purification. Ultrapure water (18.2 MΩ·cm) was used in preparing all aqueous solutions. All glassware was cleaned by aqua-regia and thoroughly rinsed by ultrapure water before nanoparticle synthesis or storage.

2.1.2 Synthesis

The silver nanoparticles are synthesized based on the Lee and Meisel method.[49] Typically, 18 mg silver nitrate salt are added into 100mL ultrapure water and brought to boiling on a hotplate. Then, 2 mL of 1% sodium citrate solution are added into the boiling solution as reductant. The reaction temperature is kept at ~85 °C for 45 minutes and then cool to room temperature before storage at 4 °C until further use. The final product is a greenish yellow colloidal solution.

2.1.3 SERS measurements

A C12710 portable Raman module (Hamamatsu Photonics, NJ.) is used for all SERS measurements. A “mix and detect” protocol is streamlined to involve minimal preparation and simple instrument training, as shown in **Figure 2**.

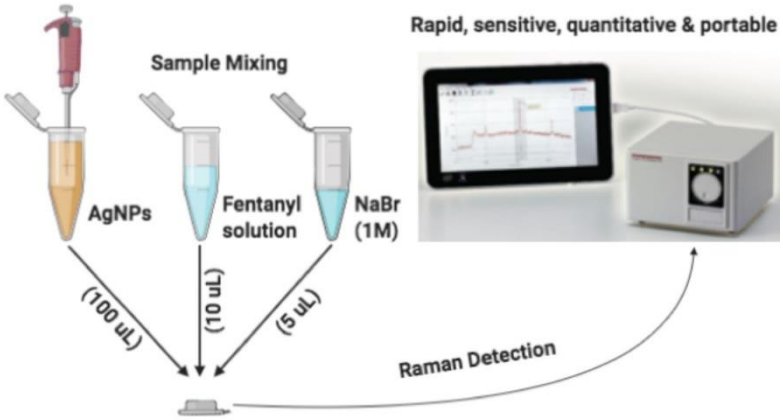

Figure 2. Scheme of the SERS-based quantitative drug analysis by coupling AgNPs with a compact and portable Raman module.

Typically, 100 μL of the AuNPs colloids (Abs. ~0.6; ~0.44 nM) are well mixed with 10 μL analyte solution in a plastic cap with 1 cm diameter which includes a matched aluminum foil piece lining on the bottom of the cap to prevent signal interference from the cap material (polypropylene). Then 5 μL of salt solution are added into the above mixture before measurement. Spectrometer calibration is carried out before the detection through the Si phonon peak at ~522 cm^{-1} of a clean silicon wafer. The proper focus for Raman measurement of solutions is achieved by tuning the focus knob and acquiring Raman signals from ~100 μL ethanol solution until maximum signal at 880 cm^{-1} is obtained. The C12710 portable Raman module employed has a 785 nm laser with a maximum power (HI mode) of 50 mW for excitation, corresponding to 6.4 $\times 10^4$ W/cm^2.

2.1.4 Salting optimization and validation

Several sodium salts are used to optimize the performance, measured in term of SERS enhancement (100 μL AgNP colloid; 10 μL, 100 nM crystal violet solution; 5 μL of salt solution: 1 M for NaCl, NaBr, NaI and 0.5 M for Na_2SO_4; 2s acquisition time on HI power mode, 785 nm lase). According to the results of the salt optimization process, NaBr is chosen in a series of concentrations (0.25 M; 0.5 M; 1 M; 2 M) for assessing optimal salt concentration, while keeping all other conditions constant. Crystal violet is used as reporter molecule for initial optimization studies due to its high Raman cross section and well

characterized spectrum. Raman signals are acquired immediately after adding 5 μL of salt solution into the mixture and then 160 spectra are collected consecutively with 2 seconds per acquisition. Crystal violet with series of concentration (50 nM; 100 nM; 200 nM; 500 nM, 1 μM) is used in the condition of NaBr salt (5 μL, 1M) to validate the detection sensitivity. A consecutive 1800 spectra are collected in 200 nM crystal violet for validation of signal stability.

2.1.5 Fentanyl detection

The same protocol as described above is used (HI power mode laser; 2 seconds acquisition time; 80 spectra) for different concentrations of fentanyl in laced recreational drugs (heroin; THC). The amount of fentanyl in drugs is represented by mass percent. For example, a 0.1% fentanyl solution in heroin is made by mixing 1 μL fentanyl (1 μg/mL) with 10 μL heroin (100 μg/mL).

2.2 Results and Discussion

2.2.1 Synthesis and characterizations

Synthesis and characterizations of AgNPs with irregular shapes are completed first. As shown in **Figure 3**, an average size of ~40 nm in diameter of the nanoparticles is characterized by TEM micrographs, also confirmed by the DLS size measurement below. These nanoparticles have a negative zeta-potential ($\zeta \sim -30.7$ mV), implying a citrate-coated surface that stabilizes the particles. The synthesized nanoparticles are also characterized by UV-Vis and showed an absorption maximum at 409 nm. After four month of storage, the UV-Vis spectrum remains unchanged, suggesting a long-term stability in nanoparticle colloidal phase for at least 4 months. Colloidal AgNPs are stable, and produce negligible SERS signals in the presence of target molecules, while displaying a well-established SERS enhancement after aggregation. Upon addition of alkali halides salt, citrate molecules on AgNPs surface are displaced by halide anions, disrupting colloidal stability and changing the color from yellow to dark green

within minutes. Subsequently, small aggregates are formed, trapping target molecules nearby and enhancing their Raman signals.

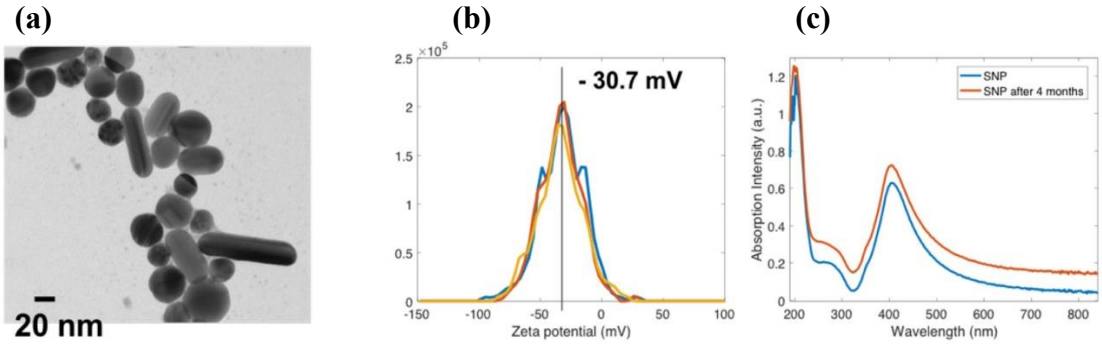

Figure 3. (a) TEM image of as-synthesized AgNPs; **(b)** zeta-potential measurements of the synthesized AgNPs; **(c)** UV-Vis absorption profiles of AgNPs before SERS measurement (blue curve) and AgNPs after 4 months of storage (red curve).

2.2.2 Aggregation dynamics

As aggregation occurs, small aggregates grow in size and eventually precipitate, leading to a dynamic SERS signal during the whole process. In order to determine a proper time window for collecting stable and reproducible signals, the aggregation dynamics of AgNPs after salting are investigated. In **Figure 4** (a), the spectra of time-dependent UV-Vis absorption shows a steep decrease for the absorption at ~409 nm (dipole mode) and increase at >800 nm (multipole modes), confirming the formation of small nanoclusters within 2~3 minutes after salting. After the 3-minute mark, the absorption peaks of both dipole and multipole slowly decline, indicating that the small nanoclusters continually grow into larger aggregates. Time-dependent size measurement data from DLS in **Figure 4** (b) further verify the formation of small nanoclusters after salting with the sudden raise in size. The AgNPs are measured to be ~38 nm in diameter prior to adding salt (similar to the ~40 nm in TEM). Then the size increases to ~1000 nm after two minutes of salting and the nanoclusters continue to grow in size before eventual precipitation.

The Raman signal after aggregation need to be stable within the time window for the quantitative detection. A SERS heatmap (150 spectra; totally 5 min acquisition) of AgNPs colloids mixed with a reporter (crystal violet, 200 nM, 10 μL) is shown in **Figure 5**,

supporting the stability of SERS signals for at least five minutes after salting, despite the uncontrollable nature of the aggregation dynamics. Hence, the first three minutes are selected to be the optimal time window for signal collection due to the domination of small nanoclusters formation and the signals stability.

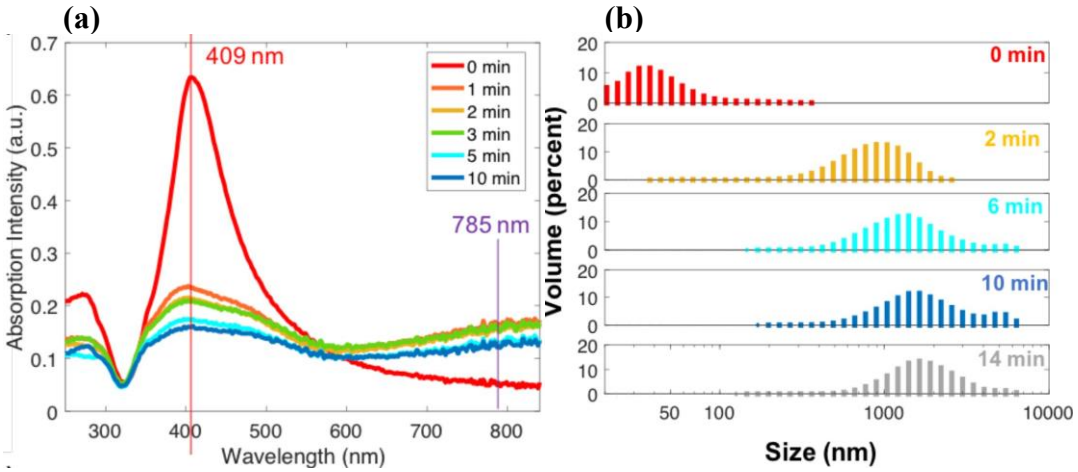

Figure 4. (a) UV-Vis absorption of the AgNP colloids (1 mL) and its temporal development after salt addition (NaBr: 1 M, 50 µL); **(b)** DLS size measurements of the AgNP colloids before and after salt addition with color codes corresponding to those in (a).

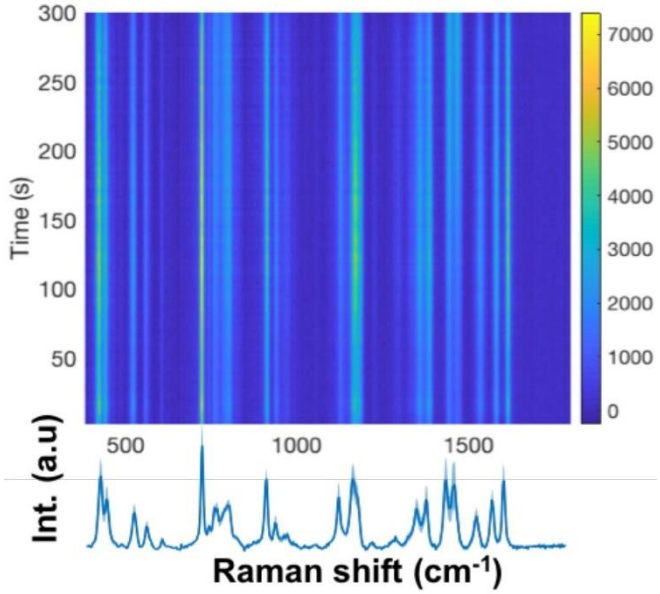

Figure 5. SERS heatmap (n=150) of AgNPs colloids mixed with a Raman reporter (crystal violet, 200 nM, 10 µL) obtained within 5 minutes. Raman heatmaps are displayed in pseudo-colors correlated with Raman intensities. The averaged SERS spectrum is aligned at the bottom of the map with the shaded region indicating the standard deviations across the mean spectrum.

2.2.3 Salting optimization

In the process of aggregation, the interactions between target molecules and nanoparticles highly depend on the salt reagents and concentrations, which means that by optimizing the salting conditions the assay performance can be improved. Various salt species and salt concentrations are applied for generating SERS signals in order to determine the proper salting condition. Crystal violet is used as a representative Raman reporter because the tertiary amine groups and benzene ring in crystal violet are similar to fentanyl and other opioids, mediating the surface interactions of negatively charged nanoparticles in a comparable fashion. As shown in **Figure 6**, NaBr has a better SERS performance compared to other salt species (NaCl, NaI, and Na_2SO_4), suggesting that bromide anions are preferable for mediating surface interactions between AgNPs and target molecules.

Figure 7 (a) displays the SERS spectra from the mixture of AgNPs and crystal violet after adding various concentration of NaBr salt. In the spectral regions of the red dashed boxes, the peak intensities are strong and stable when 0.5 M and 1 M NaBr salting are applied. **Figure 7** (b) shows a quantitative spectral analysis on a characteristic peak of crystal violet at 912 cm^{-1} (assigned to the ring breathing vibrational mode), fitting the selected Raman band. Although the fitted peak intensities reach a plateau at 0.5 M NaBr, the optimal salt concentration is selected as 1 M NaBr due to the associated signal stability, revealed by the low relative standard deviation (RSD) of the fitted peak intensity. Therefore, an optimized assay of detection for the portable SERS platform is obtained, in which NaBr is chosen as the aggregation-inducing reagent while the optimal salting conditions (1 M NaBr) and readout time window (~3 minutes) are set.

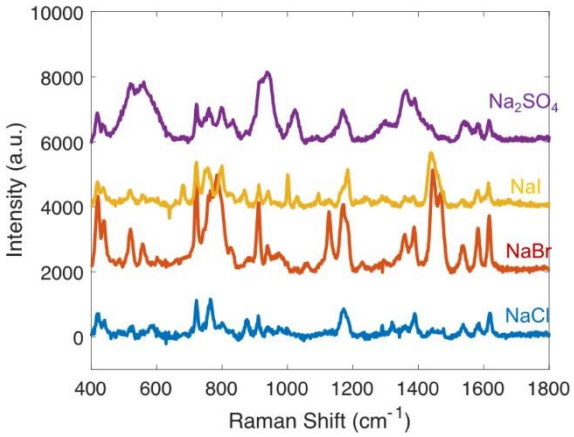

Figure 6. Averaged SERS spectra (n=40 for each concentration) acquired by mixing different salt solutions (1 M for NaCl, NaBr, NaI and 0.5 M for Na_2SO_4) with AgNPs colloids (Abs. at 409 nm, ~0.6) and crystal violet (100 nM). SERS spectra are offset for clarity.

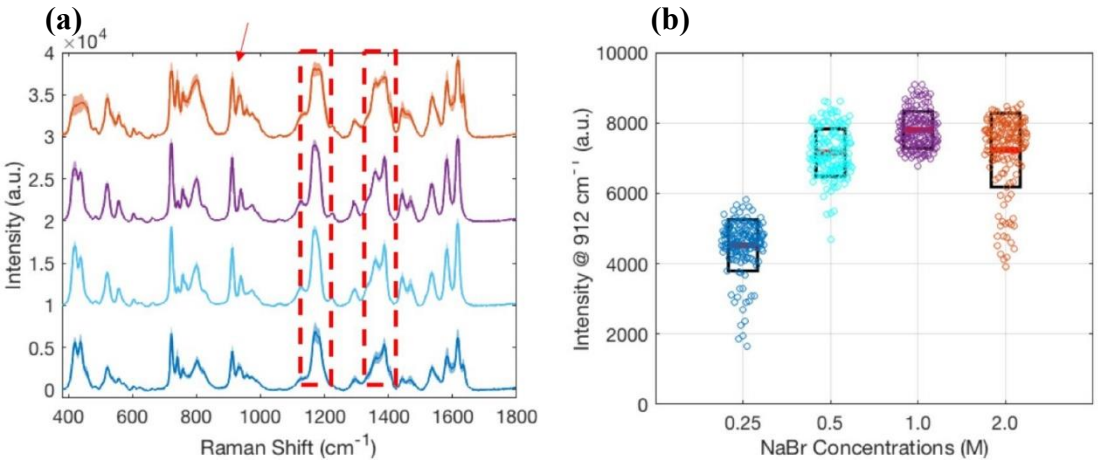

Figure 7. (a) Salt concentration optimization: Averaged SERS spectra (n=160) acquired by varying the NaBr salt concentration (blue: 0.25 M; cyan: 0.5 M; purple: 1 M; orange: 2 M) added into the mixture of AgNPs colloids and Raman reporter solution (crystal violet, 1 μM). Spectra are offset for clarity and the shaded regions of the spectra represent one standard deviation (1 σ) of the signal across the spectrum, the red arrow (at 912 cm^{-1}) and red dashed indicates the signature Raman peaks used for analysis; **(b)** Fitted peak intensities of the 912 cm^{-1} Raman band obtained from each NaBr concentration with the color codes corresponding to those used in (a). The red line is the mean of fitted peak intensities; the black box indicates the standard deviation (±1 σ).

2.2.4 Fentanyl detection

The optimized assay above is applied to trace fentanyl detection. Trace fentanyl analysis in urine and recreational drugs are essential for determining the cause of death by overdose and the on-site tracking of fentanyl respectively. Concentration-dependent SERS spectra of fentanyl spiked in urine control (artificial urine with constituents mimicking human urine) and recreational drugs (heroin; THC) are collected in the following section.

The average SERS spectra of different fentanyl concentrations spiked in urine control are compared in **Figure 8** (a). At low fentanyl concentration (0~20 ng/mL), a broad peak at ~784 cm^{-1}, a peak at 1127 cm^{-1}, and two peaks near ~1445 cm^{-1} are observed (attributed by black circles), illustrating the domination of the vibrational modes from surface anionic species such as bromide and citrate residues. When the fentanyl concentration increases, the vibrational modes of fentanyl gradually arise. Characteristic fentanyl vibrations at 828 cm^{-1}, 1001 cm^{-1}, 1029 cm^{-1}, 1172 cm^{-1}, 1198 cm^{-1}, 1593 cm^{-1} are all observed at concentrations beyond 200 ng/mL (attributed by blue triangles).[43, 44, 50]

Two clear Raman peaks at 1127 cm^{-1} and 1001 cm^{-1} with negligible spectral cross-talk are selected for quantitative analysis, assigned to the surface anionic residues and fentanyl respectively. The use of peak ratio $\frac{I_{(1001\ \mathrm{cm^{-1}})}}{I_{(1001\ \mathrm{cm^{-1}})}+I_{(1127\ \mathrm{cm^{-1}})}}$ for quantitative analysis allows us to minimize batch to batch signal variation stemmed from the instrument and the stochastic nature of nanoparticles aggregation. **Figure 8** (b) shows the plot of peak ratio against fentanyl concentration, which can be fitted well with a Langmuir type isotherm (coefficient of determination R^2=0.8894). With fentanyl concentration increase, more fentanyl molecules are present in the mixture to replace anionic residues on the nanoparticles surface through the Langmuir type adsorption behavior, suggesting a competitive adsorption process. Beyond 500 ng/mL, the Langmuir isotherm reaches a plateau and the competitive absorption of fentanyl is saturated. As shown in the inset of **Figure 8** (b), in the low concentration region from 0 to 100 ng/mL, a good linear calibration curve could be established with R^2 equal to 0.9505. The

LOD for fentanyl spiked in urine is estimated at ~5 ng/mL with a signal-to-noise ratio (s/δ) ~ 4 (where "s" is the mean of signal intensity and "δ" is the standard deviation). The detection sensitivity afforded here in the optimized portable SERS assay compares well with the immunoassays available on the market such as DRI® Fentanyl assay (ThermoFisher Scientific) which only allows qualitative mode with LOD ~2 ng/mL.

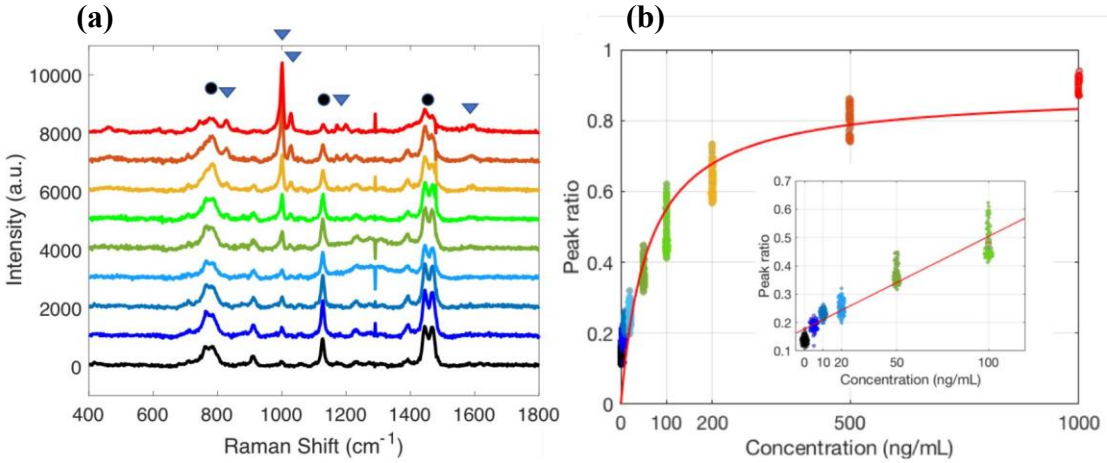

Figure 8. (a) Averaged SERS spectra (n=80) stacked in the order of increasing concentration of fentanyl spiked in urine control (0, 5, 10, 20, 50, 100, 200, 500, 1000 ng/mL). The blue triangles are peaks attributed to fentanyl and black circles attributed to surface anions. The spectra are offset for clarity; **(b)** Quantitative analysis using the peak ratios between fentanyl (1001 cm^{-1}) and surface anions (1127 cm^{-1}) plotted against the concentration. Color codes correspond to those used in (a). A Langmuir isotherm (solid red line) is used to fit the data of the entire concentration range and a linear fit is used in the low concentration regime (R^2=0.8922).

Different mass concentrations of fentanyl (trace level) in heroin and THC (major component of marijuana) are produced by mixing heroin/THC stock (100 µg/mL) with fentanyl solution (1 µg/mL), simulating trace quantities of fentanyl laced in recreational drugs. **Figure 9** (a, c) show the spectral evolution as mass concentration of adulterated fentanyl increase in heroin or THC. Similar to the SERS spectra of fentanyl in urine above (Figure 8), the vibrational modes of fentanyl (e.g. 1001 cm^{-1}) slowly grow into prominence while surface anion peaks (e.g. 1127 cm^{-1}) gradually decline. Interestingly, only one weak peak at 623 cm^{-1} for heroin and no

peak for THC is observed despite the high concentration (50 μg/mL) of heroin and THC is presented, compared with the concentration of fentanyl, which might be the result of vastly different absorption affinity toward the nanoparticles surface for fentanyl, heroin and THC. Although previous studies have proposed that C=C or carbonyl groups on opiates can facilitate the drug-Ag interaction,[51] the results obtained here appear to suggest that amine groups may also play a role in modulating the molecular adsorption affinity to the nanoparticles.

Nonetheless, quantitative analysis of the spectral response from trace fentanyl, shown in **Figure 9** (b, d), reveals a similar Langmuir type adsorption profile and a linear calibration curve in the low mass concentration range. The analysis also yields LODs at ~0.05% (5 ng in 10 μg total) and ~ 0.1% (10 ng in 10 μg total) for trace fentanyl in laced heroin and THC, respectively. The LODs achieved here are at least a magnitude lower than previous report.[44]

2.3 Conclusion

In summary, a portable SERS assay based on AgNPs colloidal aggregation is optimized for rapid, sensitive, and quantitative detection of fentanyl in trace amounts. NaBr salt solution with concentration of 1 M and the 3 minutes readout window are the optimal conditions for inducing AgNPs aggregation and optimized detection. The optimized assay supports a LOD of ~5 ng/mL for fentanyl spiked in urine controls and a LOD of ~0.1 % (10 ng in 10 μg total) mass percent for fentanyl in laced recreational drugs such as heroin or THC. The sensitivity achieved here suggests a great potential for application in clinical detection of drug overdose, as the concentration of fentanyl in biofluids are expected to be within 3~300 ng/mL for intoxicated or acutely overdosed individuals. Although other opioid drugs such as heroin and THC cannot be well detected and quantitated, the observation that drug-Ag interaction mediated by amine groups implies a possible way to improve opioid detection in portable SERS for future studies.

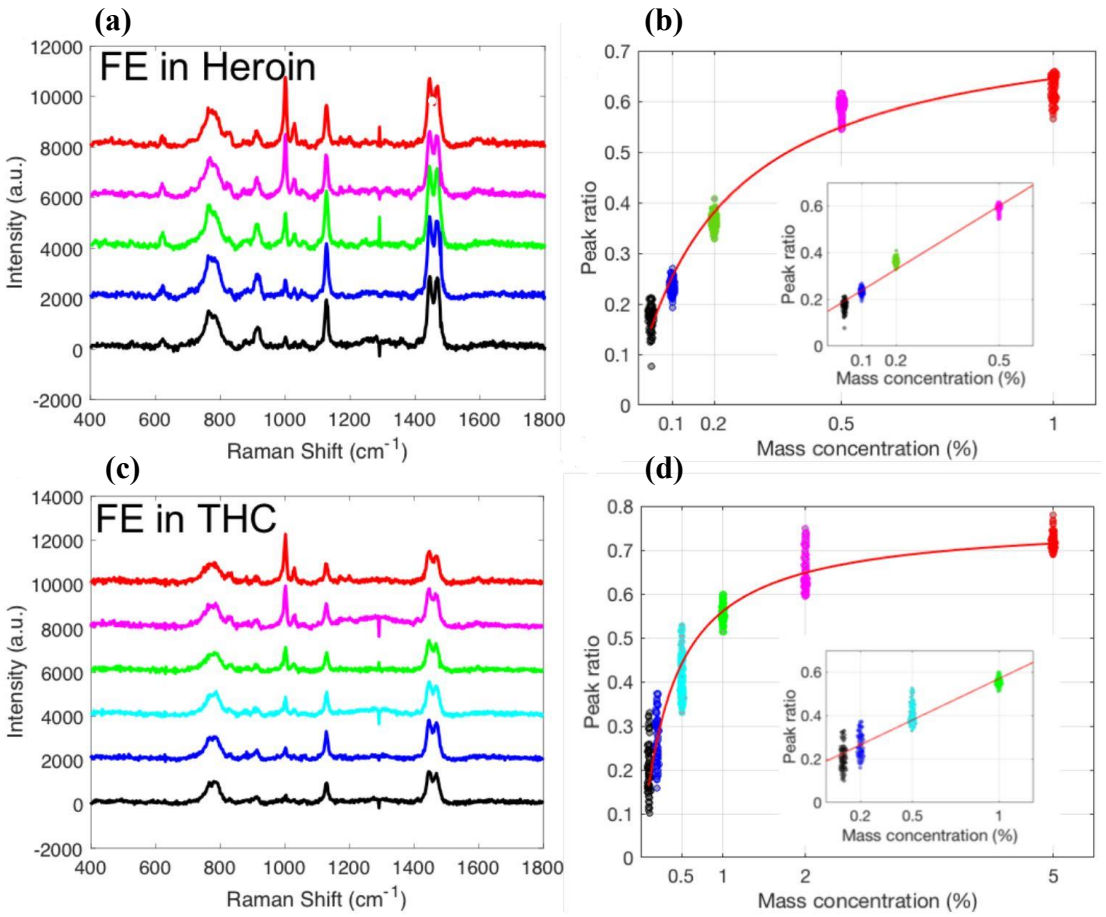

Figure 9. (a, c) Averaged SERS spectra (n=80) stacked in order of increasing mass concentrations of fentanyl mixed in heroin (a) or THC (c); **(b, d)** Quantitative analysis using the peak ratios between fentanyl (1001 cm^{-1}) and anionic residues (1127 cm^{-1}) with the same color codes as those in (a) or (c). A Langmuir isotherm (solid red line) is used to fit the entire data range and a linear fit used in the low concentration region [R^2=0.9677 in (b), R^2=0.8673 in (d)].

Chapter 3 Improving the Sensitivity of Gold Molecular Beacons

Gold nanoparticle-based molecular beacons (MB-AuNPs) are the variants of spherical nucleic acids in which many hairpin-like single-stranded self-hybridized oligonucleotides are immobilized on the surface of AuNPs. These oligonucleotides are labelled with fluorophore and quencher (AuNPs), which hold an internal fluorescence recovering property due to their ability to undergo a conformational transition when binding to oligonucleotide targets.[52] Molecular beacons (MBs) present many potential advantages as a tool in molecular biology, clinical diagnostics, and analytical chemistry. The detection of micro-RNA or oncogenes and the multiplexed analysis of other biomarkers have been explored by other researchers, often however with inconsistent results.[34, 53-57] However, the sensitivity and specificity of MBs are still limited and the effects of conformations and surrounding environment on MBs performance are still ambiguous. According to thermodynamic analyses, hairpin-like oligonucleotides with a stem-loop structure can exist in three different states: 1) Hybridized to the targets, 2) in a self-hybridized hairpin structure, or 3) free in a random coil.[58] Different factors such as incubation temperature, targets, or the surrounding ions will variably affect the conformational state of these oligonucleotides. Moreover, the density of hairpin probes on the AuNPs surface plays an essential role in the performance of MB-AuNPs for target detection and a short and simple single strand DNA (e.g. T_{10}) is usually used as a "spacer" for optimizing the performance by reducing steric hindrance and facilitating the hybridization of the probes with their targets.[34]

Herein, I will demonstrate how fluorescence recovery is achieved when incubating the MBs with their perfectly complementary targets, which leads to the removal of the fluorophore away from the AuNP surface due to the opening of the hairpin structure. In order to improve the sensitivity of target detection, the effects of temperature, molar ratio of particles to MBs and MBs to spacer (T_{10}) are investigated. Based on the fluorescence enhancement, the molar ratio of 1000/1 for MBs plus T_{10} to gold nanoparticles leads to a relatively strong and stable

signal enhancement. And the ratio of MBs to T_{10} is examined within the range of 3~5, indicating relatively less influence on the result. Calibration curves for the detection are generated under different concentration of targets, indicating a LOD of ~10 nM for room temperature detection and a LOD of ~20 nM at 37.5 ℃.

3.1 Materials and Method

3.1.1 Materials

Tetrachloroauric (III) acid trihydrate ($HAuCl_4 \cdot 3H_2O$; ≥ 99%), trisodium citrate dihydrate ($Na_3C_6H_5O_7 \cdot 2H_2O$), Tris(2-carboxyethyl) phosphine hydrochloride (TCEP, $C_9H_{15}O_6P \cdot HCl$), sodium dodecyl sulfate (SDS, $C_{12}H_{25}NaO_4S$; ≥ 99%), phosphate buffer solution (PB buffer; 1.0 M; pH 7.4, 25 °C), phosphate-buffered saline (PBS; 1×; pH 7.4, 25 °C), sodium chloride (NaCl; ≥99.5%). All these chemicals were used without further purification. Ultrapure water (18.2 MΩ·cm) was used in preparing all aqueous solutions. All glassware was cleaned by aqua-regia and thoroughly rinsed by ultrapure water before nanoparticle synthesis or storage.

Gene PB2, corresponding to polymerase basic protein 2 usually found in influenza A virus, is chosen here as the target segment to test the MB-AuNPs probe. The target PB2 sequence is 5'-CAG GAA GAC AGG AGA AGA CTG AGG-3'. The beacon probe is determined for facilitating the conformational transition. The beacon sequence is 5'-FAM-CG TCA CTC AGT CTT CTC CTG TCT TCC TTG ACG (T_{10}) -Thiol-3'. As for the control experiments, the random sequence 5'-CGT GCC CAG TGA GCG AGG ACT GCA-3' is employed.

3.1.2 Synthesis of gold nanoparticles

Gold nanoparticles (AuNPs) are synthesized according to a modified synthesis described by Turkevich *et al*.[59] Typically, 8 mL of 0.025 M $HAuCl_4$ salt are added into 477 mL of ultrapure water. The diluted gold salt solution is heated up and bought to a boil under gentle stirring. Then 15 mL of 1% citric acid trisodium solution is added to the boiling solution and

kept boiling for 5 minutes before cooling to room temperature. The cooled product is purified by centrifugation at 6000 g for 45 minutes. The nanospheres are collected from the sediments at the bottom of the centrifuge tube and resuspend in water. The final product is a deep red colloidal solution.

3.1.3 Preparation of MB-AuNPs

Several molar ratios are used in order to optimize the performance of MB-AuNPs. The molar ratio of the MBs to the T_{10} is selected as 3:1 and 5:1. The molar ratios of the beacon plus the spacer (MB+ T_{10}) to the gold nanoparticles (AuNPs) are chosen as 200:1, 500:1 and 1000:1. The AuNPs colloidal solution is diluted and the UV-Vis absorptance (Abs) is measured at a 1 mm path length. The final concentration for AuNPs colloidal solution is set at 2.45 nM, calculated by Beer-Lambert law where Abs ~ 0.1 and molar extinction coefficient $\varepsilon = 4.08\times10^{8}$ $mol^{-1}\bullet cm^{-1}$ for AuNPs with ~20 nm diameter.

The beacons and spacers are anchored on the gold nanoparticles surface through a modified protocol based on previous reports.[60] Typically, when the molar ratio of MB to T_{10} is equal to 3:1 and MB+ T_{10} to AuNPs is equal to 1000:1, 18.4 μL of MB solution (100 μM) is mixed with 6.1 μL of T_{10} solution (100 μM) and heated to 65 °C, incubated for 10 minutes then cooled to room temperature. 122.5 μL of TCEP (10 mM) are then added into the MB+ T_{10} solution before incubation for 3 hours at room temperature. Afterwards, 853 μL of AuNPs colloidal solution (Abs ~ 0.12) are added into the mixture, leading to a final AuNPs solution with absorption ~ 0.1, followed by a 16 hours incubation in the dark. Then 10 μL of SDS solution (10% mass fraction) and 100 μL of PB buffer (0.1 M) are added sequentially into the mixture and allowed a 10 minutes incubation. Six aliquots of 20 μL of NaCl (2 M) are then added every 30 minutes, and the reaction is allowed to proceed for another 16 hours incubation at room temperature in the dark. The products are purified by centrifugation at 13000 rpm for 13 minutes and washed with PBS, repeated three times. The final products are stored at 4 °C until further use.

3.1.4 Fluorescence measurement

A fluorescence kinetics is measured at 475 nm absorption and 525 nm emission, collecting signals every 30 seconds. For a typical fluorescence measurement, 100 μL of MB-AuNPs solution (Abs~0.04) are added into a black microwell plate. After a 10 minutes base measurement, 5 μL of 10 μM target solution are added into the microwell for a final target concentration of 500 nM, followed by a 60 minutes kinetics fluorescence measurement. Every measurement is carried out at a fixed temperature (either 25 °C or 37.5 °C).

3.2 Results and Discussion

3.2.1 Syntheses and characterizations

A characteristic absorption peak at 523 nm for the gold nanoparticles (AuNPs) is observed via UV-Vis analysis, shown in **Figure 10**, corresponding to a particle size of around 23 nm in diameter according to previous reports.[61] The size of the prepared AuNPs is also confirmed by the DLS size measurements at room temperature (25°C), shown below in **Figure 11**, indicating an average size of 22.8 (± 6.4 σ) nm in diameter.

After the immobilization of MBs and T_{10} on the surface of AuNPs, forming the probes particles MB-AuNPs, the particle size will increase due to the added layer of beacon oligonucleotides and spacers. Although the red shift for size increase in the UV-Vis absorptance is negligible, only 3 nm red shift for the size increase from 20 to 30 nm in diameter, the size measurement from DLS can still reflect the increase in size for MB-AuNPs, indicating an average size of 31.2 (± 9.9 σ) nm in diameter (**Figure 11**, MB-AuNPs). When the target oligonucleotides are presented and hybridize with the MBs, the fluorophores in the MBs are pushed away from the surface due to the conformational transition of the MBs hairpin structure into an extended double strand. As a result, the particle size increases after incubation with targets, revealed by the DLS measurement of an average size of 49.3 (± 17.4 σ) nm in diameter (**Figure 11**, MB-AuNPs+ Targets).

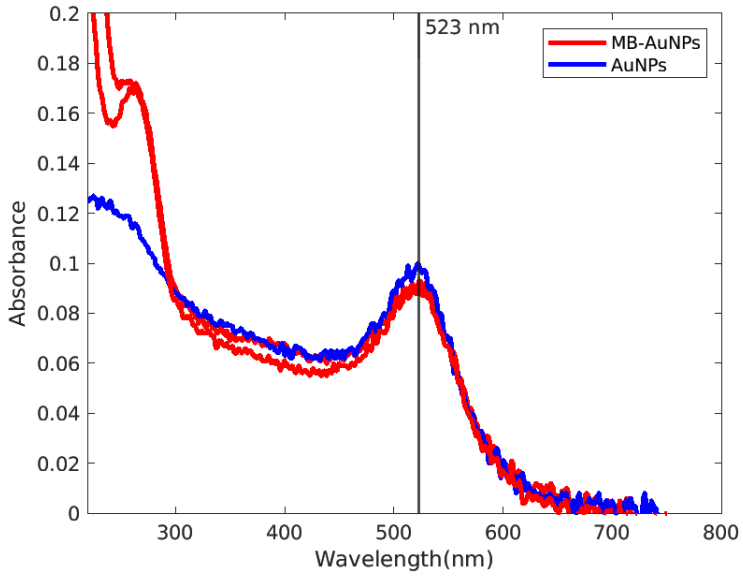

Figure 10. UV-Vis absorption of the AuNPs colloids (blue line) and the MB-AuNPs with both 3:1 and 5:1 molar ratio of MBs to T_{10}, when the molar ratio of (MB+ T_{10})/ AuNPs equal to 1000 (red line).

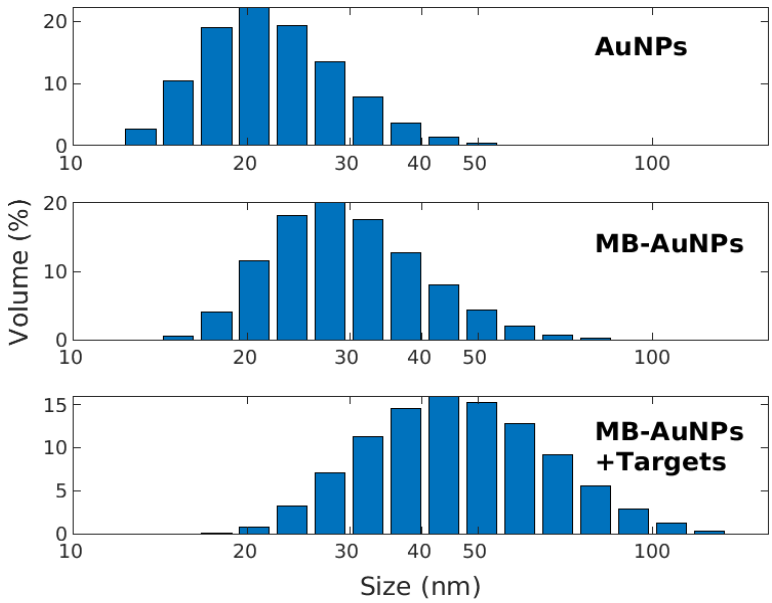

Figure 11. DLS size measurements of the AuNPs colloids (top panel), the MB-AuNPs with 3:1 molar ratio of MBs to T_{10}, where the molar ratio of (MB+ T_{10})/ AuNPs is equal to 1000 (middle panel), and the MB-AuNPs after incubation in the presence of 500 nM targets (bottom panel).

3.2.2 Fluorescence kinetics

In the preparation of MB-AuNPs, the molar ratio of surface oligonucleotides (MB and T_{10}) to AuNPs determines the amount of oligonucleotides immobilized on each particle, altering the performance and the degree of fluorescence recovery. Theoretically, when the molar ratio of (MB+ T_{10})/ AuNPs increases, the final fluorescence recovery should increase on account of the increased amount of fluorophore per particle. But there would be a maximum fluorescent signal for recovery, due to the saturation of oligonucleotides on the particle surface. In addition, the molar ratio of MBs to T_{10} affects the distribution of MB oligonucleotides on the surface. The increase of T_{10} fraction would reduce crowding of MB oligonucleotides while creating more space between the hairpin MBs, thus lowering the steric hindrance for hybridization with targets, and leading to an increase of fluorescence recovery. However, when the oligonucleotides are saturated on the surface of particles, the increase of T_{10} would compete with the MBs and reduce the amount of MBs on the surface, resulting in a final decrease of fluorescence recovery.

The preparation of MB-AuNPs is carried out with 200:1, 500:1, and 1000:1 molar ratios of (MB+ T_{10})/ AuNPs, followed by the measurement of fluorescence kinetics at 25°C, as shown in **Figure 12**. The background in **Figure 12** is subtracted according to the base measurement for better comparison. As a result, when the (MB+ T_{10})/ AuNPs increase from 200 to 1000, the fluorescence recovery increases from around 4 relative fluorescent unite (RFU) enhancement (**Figure 12,** a) to ~ 90 RFU enhancement (**Figure 12**, c), suggesting that the oligonucleotides on particle surface have not reached saturation while presenting a desirable recovery when (MB+ T_{10})/ AuNPs equal to 1000:1. Meanwhile, the fluorescence recovery of 3:1 molar ratio of MBs to T_{10} is slightly higher than 5:1 (**Figure 12**, a c), indicating the positive effect of the spacers. As for the **Figure 12** (b), the abnormal fluorescence recovery in the presence of random oligonucleotides maybe because of the falling-off of MBs from the crowded MBs stacks on the surface. During the preparation of MB-AuNPs, some MBs would stack and tangle on the surface of AuNPs, forming the stacks of MBs through hydrogen

bonding and hydrophobic effect instead of thiol-gold interaction. These MBs stacks would grow because of the inadequate purification, disturbing the order of oligonucleotides distribution on the surface of particles.

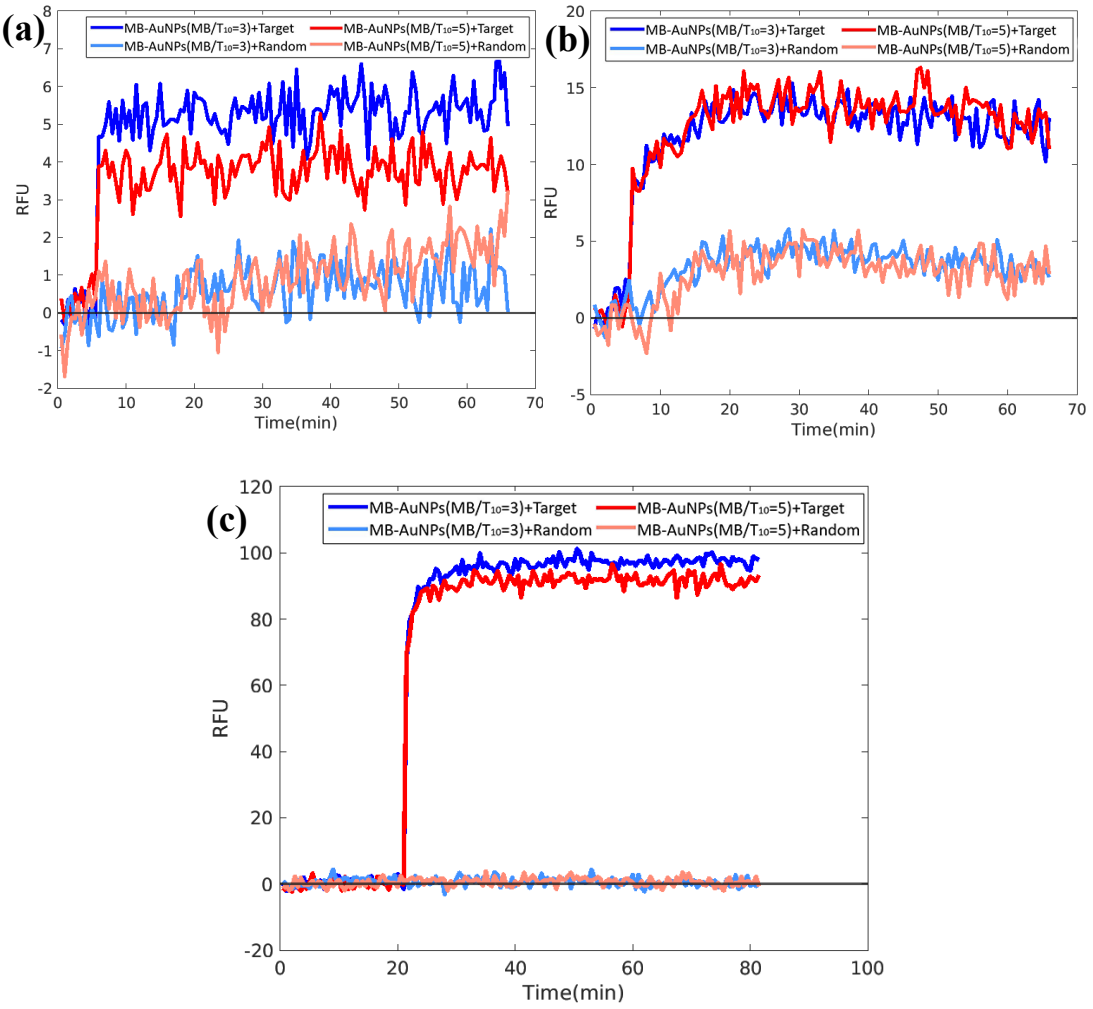

Figure 12. Fluorescence kinetics measurement for MB-AuNPs (Abs ~ 0.04) at room temperature (25°C), in which the molar ratio of (MB+ T_{10})/ AuNPs equal to 200 (a), 500 (b), 1000 (c), with both 3:1 (blue and light blue line) and 5:1 (red and light red line) molar ratio of MBs to T_{10}. Targets (blue and red line) and random oligonucleotides (light blue and light red line) are added after 5 or 20 minutes base measurement, both reaching a final concentration of 500 nM.

According to the above explored conditions for molar ratio of (MBs+ T_{10})/ AuNPs and MBs/ T_{10}, quantitative analyses of the MB-AuNPs were carried out at both room temperature and 37.5°C for estimating the potential as a practical biosensor. Concentration-dependent fluorescent recoveries of MB-AuNPs with (MBs+ T_{10})/ AuNPs= 1000 and MBs/ T_{10}= 3 are collected in **Figure 13**.

The fluorescence kinetics signals at different concentrations of targets and random oligonucleotides are compared in **Figure 13** (a) and (c). MB-AuNPs products from the same batch are exposed to 25°C (**Figure 13** a) and 37.5°C (**Figure 13** c), collecting the fluorescence signal without adding oligonucleotides in the first 10 minutes. At room temperature, the fluorescence signals are steady and reproducible in the first 10 minutes, giving the original fluorescence background of MB-AuNPs products, while at 37.5°C, the fluorescence signals are increasing but still reproducible during the first 10 minutes, indicating a gradual degradation of MB-AuNPs due to the falling-off of MBs and the conformational change of MBs hairpin structure, caused by the temperature increase. Random oligonucleotides and targets with different concentrations are added at 10 minutes. The addition of targets leads to different degrees of immediate fluorescence increase depending on the target concentrations while the fluorescence remains the same as the background when the random oligonucleotides or PBS are added. After oligonucleotide addition at 37.5°C, the fluorescence background keeps increasing gradually and reaches a plateau at around 20 minutes, suggesting the MB-AuNPs system reaches a new equilibrium at 37.5°C.

Figure 13 (b) and (d) display the quantitative analyses of fluorescence intensity after oligonucleotide addition at 25°C (**Figure 13** b) and 37.5°C (**Figure 13** d) without background subtraction, showing the real correlation between the fluorescence intensity and the target concentration. The plots for both 25°C and 37.5°C can be fitted well with a Langmuir type isotherm, with R^2=0.971 for (b) and R^2=0.934 for (d). With targets concentration increase, more target oligonucleotides are present in the mixture and available for hybridization with hairpin-like MBs on the nanoparticles surface, resembling a Langmuir type adsorption

behavior. At room temperature, the fitted curve has not reached a plateau yet, meaning that target hybridization is not saturated and there are MBs on the particles surface still available for targets recognition. On the contrary, after addition of targets at 200 nM concentration at 37.5°C, the curve reaches a plateau saturating target binding, which could verify the partial degradation of MB-AuNPs stemmed from the temperature increase.

In the inset of **Figure 13** (b) and (d), in the low target concentration regime from 10 to 200 nM, a good linear calibration curve could be established with R^2=0.92 for the inset in (b) and R^2=0.942 for the inset in (d). The analyses yield LODs at around 10 nM at room temperature and around 20 nM at 37.5°C for target oligonucleotide detection.

3.3 Conclusion

In summary, a biosensor of gold nanoparticles molecular beacons is developed and characterized, proceeding a fluorescence recovery through separation of MB fluorophores from the nanoparticle surface to detect target oligonucleotides. The molar ratio of (MBs+ T_{10})/ AuNPs= 1000 and MBs/ T_{10}= 3 for the MB-AuNPs probe are selected for a desirable fluorescence recovery. Concentration-dependent fluorescence kinetics measurements at both room temperature and 37.5°C are carried out, indicating the potential of MB-AuNPs for biomarker detection in in-vitro and intracellular assays. The quantitative analyses give a LOD of ~10 nM at room temperature and ~20 nM at 37.5°C for target oligonucleotides detection.

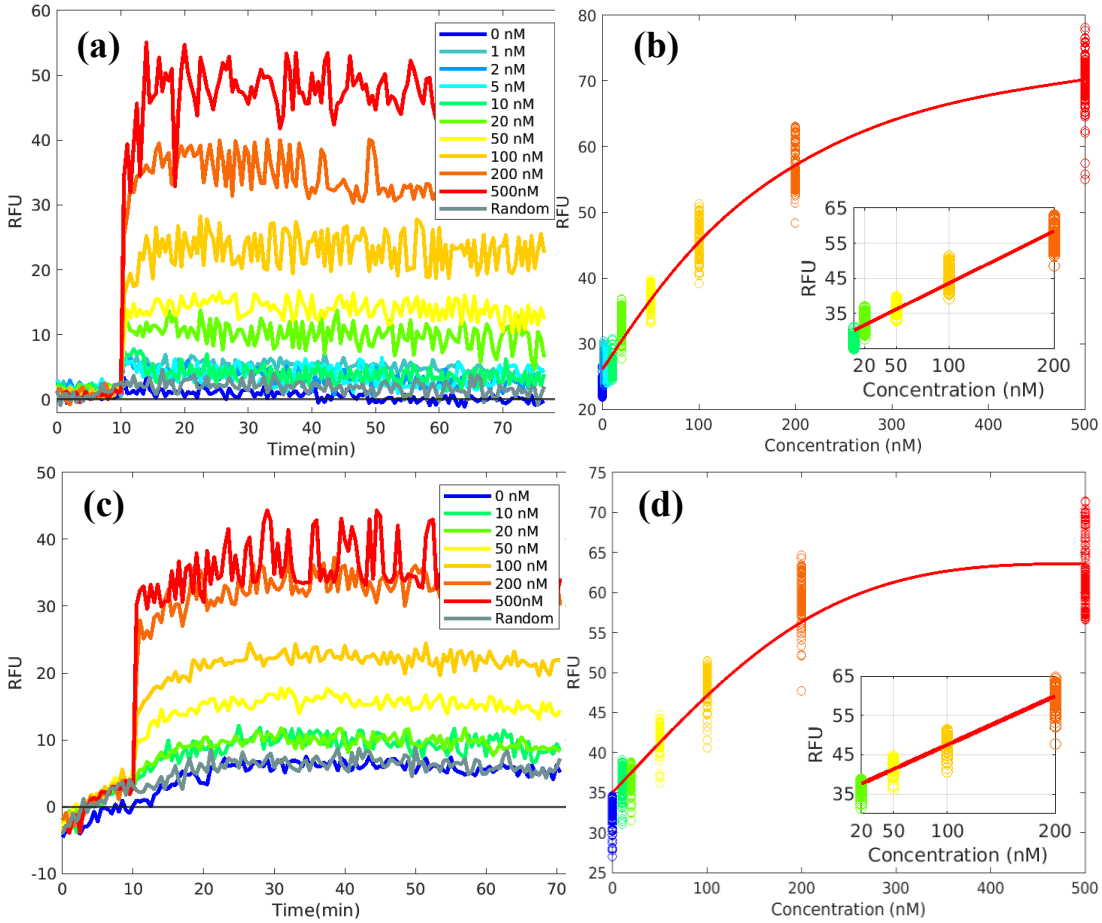

Figure 13. (a, c) Fluorescence kinetics measurements of MB-AuNPs (Abs ~ 0.04), in which the molar ratio of (MB+ T_{10})/ AuNPs=1000:1 and MBs/ T_{10} =3:1, under different targets concentrations (0, 1, 2, 5, 10, 20, 50, 100, 200, 500 nM) and random oligonucleotides (500 nM) at 25°C (a) and 37.5°C (c); **(b, d)** Quantitative analysis using the fluorescent signals collected when the complementary targets or random control are added after the first 10 minutes base measurement at 25°C (b) and 37.5°C (d). A Langmuir isotherm (red curves) is used to fit the data of the entire concentration range and a linear fit is used in the low concentration regime. Each oligonucleotide concentration is assigned to one color consistently.

Chapter 4 Conclusion

The studies in this thesis aim to improve the detection sensitivity in molecular assays by optimizing and tuning the separation of fluorophores or analytes from the surface of plasmonic nanoparticles. Solution-based assays based on sliver nanoparticle colloids and gold nanoparticle molecular beacons are used for trace drug detection and short oligonucleotide biomarkers detection, respectively.

Fentanyl molecules are trapped in the junctions between silver nanoparticles due to salting-mediated aggregation, producing a strong SERS signal from trace fentanyl molecule enabled by direct SERS detection. The conditions for aggregation are optimized to 1 M of NaBr salt solution with 3 minutes detection time window, leading to a LOD of ~5 ng/mL for fentanyl spiked in urine controls and a LOD of ~0.1 % (10 ng in 10 μg total) mass percent for fentanyl in laced recreational drugs, such as heroin or THC. On the contrary, fluorophores in hairpin-like molecular beacons are separated and pushed away from the surface of gold nanoparticles due to the hybridization of target oligonucleotides with molecular beacons, opening the hairpin-like oligonucleotide structure, resulting in a PEF signals with fluorescence recovery for indirect detection of target oligonucleotides. The conditions for developing the molecular beacons functionalized gold nanoparticles are optimized to 1000:1 and 3:1 for the molar ratio of (MBs+ T_{10})/ AuNPs and MBs/ T_{10}, respectively, giving a desirable fluorescence recovery for target detection. The quantitative analyses in different target concentrations indicate that the target oligonucleotides detection with a LOD of ~10 nM at room temperature and a LOD of ~20 nM at 37.5°C are achieved.

For future directions, the silver nanoparticle assay could be applied to some clinical samples to evaluate the potential of in-situ detection. Detection of drugs other than fentanyl could also be further developed and improved. For the other part, the distribution of MBs and spacers on the gold nanoparticle surface should be further explored. For example, the actual ratios of

MBs to gold nanoparticles and MBs to spacers could be measured by ICP-AES for further optimization. Moreover, the detection based on SERS signal change could also be further explored.

Chapter 5 References

1. Wang, J., Nanomaterial-based electrochemical biosensors. *Analyst* **2005,** *130* (4), 421-426.
2. Hu, L.; Kim, H. S.; Lee, J.-Y.; Peumans, P.; Cui, Y., Scalable coating and properties of transparent, flexible, silver nanowire electrodes. *ACS nano* **2010,** *4* (5), 2955-2963.
3. Lu, X.; Yavuz, M. S.; Tuan, H.-Y.; Korgel, B. A.; Xia, Y., Ultrathin gold nanowires can be obtained by reducing polymeric strands of oleylamine− AuCl complexes formed via aurophilic interaction. *Journal of the American Chemical Society* **2008,** *130* (28), 8900-8901.
4. Zhang, D.; Neumann, O.; Wang, H.; Yuwono, V. M.; Barhoumi, A.; Perham, M.; Hartgerink, J. D.; Wittung-Stafshede, P.; Halas, N. J., Gold nanoparticles can induce the formation of protein-based aggregates at physiological pH. *Nano Lett.* **2009,** *9* (2), 666-671.
5. Zhao, W.; Chiuman, W.; Lam, J. C.; McManus, S. A.; Chen, W.; Cui, Y.; Pelton, R.; Brook, M. A.; Li, Y., DNA aptamer folding on gold nanoparticles: from colloid chemistry to biosensors. *Journal of the American Chemical Society* **2008,** *130* (11), 3610-3618.
6. Kneipp, K.; Moskovits, M.; Kneipp, H., Surface-enhanced Raman scattering. *Physics Today* **2007,** *60* (11), 40.
7. Raman, C. V.; Krishnan, K. S., A new type of secondary radiation. *Nature* **1928,** *121* (3048), 501-502.
8. Kneipp, J.; Kneipp, H.; Kneipp, K., SERS—a single-molecule and nanoscale tool for bioanalytics. *Chemical Society Reviews* **2008,** *37* (5), 1052-1060.
9. Jones, M. R.; Osberg, K. D.; Macfarlane, R. J.; Langille, M. R.; Mirkin, C. A., Templated techniques for the synthesis and assembly of plasmonic nanostructures. *Chemical reviews* **2011,** *111* (6), 3736-3827.
10. Ringe, E.; Zhang, J.; Langille, M. R.; Sohn, K.; Cobley, C.; Au, L.; Xia, Y.; Mirkin, C. A.; Huang, J.; Marks, L. D., Effect of size, shape, composition, and support film on localized surface plasmon resonance frequency: a single particle approach applied to silver bipyramids and gold and silver nanocubes. *MRS Online Proceedings Library Archive* **2009,** *1208*.
11. Ringe, E.; Langille, M. R.; Sohn, K.; Zhang, J.; Huang, J.; Mirkin, C. A.; Van Duyne, R. P.; Marks, L. D., Plasmon length: a universal parameter to describe size effects in gold nanoparticles. *The journal of physical chemistry letters* **2012,** *3* (11), 1479-1483.
12. Ghosh, S. K.; Pal, T., Interparticle coupling effect on the surface plasmon resonance of gold nanoparticles: from theory to applications. *Chemical reviews* **2007,** *107* (11), 4797-4862.
13. Jain, P. K.; El-Sayed, M. A., Surface plasmon coupling and its universal size scaling in metal nanostructures of complex geometry: elongated particle pairs and nanosphere trimers. *The Journal of Physical Chemistry C* **2008,** *112* (13), 4954-4960.
14. Li, M.; Cushing, S. K.; Wu, N., Plasmon-enhanced optical sensors: a review. *Analyst* **2015,** *140* (2), 386-406.
15. Schatz, G. C., Theoretical studies of surface enhanced Raman scattering. *Accounts of Chemical Research* **1984,** *17* (10), 370-376.
16. Schatz, G. C.; Young, M. A.; Van Duyne, R. P., Electromagnetic mechanism of SERS. In *Surface-enhanced Raman scattering*, Springer: 2006; pp 19-45.
17. Tong, L.; Zhu, T.; Liu, Z., Approaching the electromagnetic mechanism of surface-enhanced Raman scattering: from self-assembled arrays to individual gold nanoparticles. *Chemical Society Reviews* **2011,** *40* (3), 1296-1304.

18. Ameer, F. S.; Hu, W.; Ansar, S. M.; Siriwardana, K.; Collier, W. E.; Zou, S.; Zhang, D., Robust and reproducible quantification of SERS enhancement factors using a combination of time-resolved Raman spectroscopy and solvent internal reference method. *The Journal of Physical Chemistry C* **2013,** *117* (7), 3483-3488.
19. Lakowicz, J. R., Radiative decay engineering 5: metal-enhanced fluorescence and plasmon emission. *Anal. Biochem.* **2005,** *337* (2), 171-194.
20. Lakowicz, J. R., *Principles of fluorescence spectroscopy*. Springer Science & Business Media: 2013.
21. Tsai, Y.; Lin, C.; Chang, J., Controlling spontaneous emission with the local density of states of honeycomb photonic crystals. *Optical review* **2009,** *16* (3), 347-350.
22. Khurgin, J.; Sun, G., Enhancement of optical properties of nanoscaled objects by metal nanoparticles. *JOSA B* **2009,** *26* (12), B83-B95.
23. Mertens, H.; Koenderink, A.; Polman, A., Plasmon-enhanced luminescence near noble-metal nanospheres: Comparison of exact theory and an improved Gersten and Nitzan model. *Physical Review B* **2007,** *76* (11), 115123.
24. Sun, G.; Khurgin, J. B.; Yang, C., Impact of high-order surface plasmon modes of metal nanoparticles on enhancement of optical emission. *Appl. Phys. Lett.* **2009,** *95* (17), 171103.
25. Bharadwaj, P.; Novotny, L., Spectral dependence of single molecule fluorescence enhancement. *Opt. Express* **2007,** *15* (21), 14266-14274.
26. Kang, K. A.; Wang, J.; Jasinski, J. B.; Achilefu, S., Fluorescence manipulation by gold nanoparticles: from complete quenching to extensive enhancement. *Journal of nanobiotechnology* **2011,** *9* (1), 16.
27. Alvarez-Puebla, R.; Liz-Marzán, L. M.; García de Abajo, F. J., Light concentration at the nanometer scale. *The Journal of Physical Chemistry Letters* **2010,** *1* (16), 2428-2434.
28. Solís, D. M.; Taboada, J. M.; Obelleiro, F.; Liz-Marzán, L. M.; García de Abajo, F. J., Optimization of nanoparticle-based SERS substrates through large-scale realistic simulations. *ACS photonics* **2017,** *4* (2), 329-337.
29. Chen, G.; Wang, Y.; Yang, M.; Xu, J.; Goh, S. J.; Pan, M.; Chen, H., Measuring ensemble-averaged surface-enhanced Raman scattering in the hotspots of colloidal nanoparticle dimers and trimers. *Journal of the American Chemical Society* **2010,** *132* (11), 3644-3645.
30. Bell, S. E.; Sirimuthu, N. M., Surface-enhanced Raman spectroscopy (SERS) for sub-micromolar detection of DNA/RNA mononucleotides. *Journal of the American Chemical Society* **2006,** *128* (49), 15580-15581.
31. Liu, J.; Cao, Z.; Lu, Y., Functional nucleic acid sensors. *Chemical reviews* **2009,** *109* (5), 1948-1998.
32. Rosi, N. L.; Giljohann, D. A.; Thaxton, C. S.; Lytton-Jean, A. K.; Han, M. S.; Mirkin, C. A., Oligonucleotide-modified gold nanoparticles for intracellular gene regulation. *Science* **2006,** *312* (5776), 1027-1030.
33. Jayagopal, A.; Halfpenny, K. C.; Perez, J. W.; Wright, D. W., Hairpin DNA-functionalized gold colloids for the imaging of mRNA in live cells. *Journal of the American Chemical Society* **2010,** *132* (28), 9789-9796.
34. Uddin, M. I.; Jayagopal, A.; Wong, A.; McCollum, G. W.; Wright, D. W.; Penn, J. S., Real-time imaging of VCAM-1 mRNA in TNF-α activated retinal microvascular endothelial cells using antisense hairpin-DNA functionalized gold nanoparticles. *Nanomed. Nanotechnol. Biol. Med.* **2018,** *14* (1), 63-71.
35. Spencer, M. R.; Warner, M.; Bastian, B. A.; Trinidad, J. P.; Hedegaard, H., Drug overdose deaths involving fentanyl, 2011-2016. *National vital statistics reports: from the Centers for Disease Control and Prevention, National Center for Health Statistics, National Vital Statistics System* **2019,** *68* (3), 1-19.
36. Miller, L. N.; Mercer, S. L., Drugs of abuse and addiction: an integrated approach to teaching. *Currents in Pharmacy Teaching and Learning* **2017,** *9* (3), 405-414.
37. Gu, X.; Trujillo, M. J.; Olson, J. E.; Camden, J. P., SERS sensors: recent

developments and a generalized classification scheme based on the signal origin. *Annual Review of Analytical Chemistry* **2018,** *11*, 147-169.

38. Indrasekara, A. D. S.; Meyers, S.; Shubeita, S.; Feldman, L. C.; Gustafsson, T.; Fabris, L., Gold nanostar substrates for SERS-based chemical sensing in the femtomolar regime. *Nanoscale* **2014,** *6* (15), 8891-8899.
39. Chen, H.-Y.; Lin, M.-H.; Wang, C.-Y.; Chang, Y.-M.; Gwo, S., Large-scale hot spot engineering for quantitative SERS at the single-molecule scale. *Journal of the American Chemical Society* **2015,** *137* (42), 13698-13705.
40. Wu, H.-Y.; Cunningham, B. T., Point-of-care detection and real-time monitoring of intravenously delivered drugs via tubing with an integrated SERS sensor. *Nanoscale* **2014,** *6* (10), 5162-5171.
41. Shende, C.; Brouillette, C.; Farquharson, S., Detection of codeine and fentanyl in saliva, blood plasma and whole blood in 5-minutes using a SERS flow-separation strip. *Analyst* **2019,** *144* (18), 5449-5454.
42. Wei, W. Y.; White, I. M., Inkjet-printed paper-based SERS dipsticks and swabs for trace chemical detection. *Analyst* **2013,** *138* (4), 1020-1025.
43. Fedick, P. W.; Bills, B. J.; Manicke, N. E.; Cooks, R. G., Forensic sampling and analysis from a single substrate: surface-enhanced raman spectroscopy followed by paper spray mass spectrometry. *Anal. Chem.* **2017,** *89* (20), 10973-10979.
44. Haddad, A.; Comanescu, M. A.; Green, O.; Kubic, T. A.; Lombardi, J. R., Detection and quantitation of trace fentanyl in heroin by surface-enhanced Raman spectroscopy. *Anal. Chem.* **2018,** *90* (21), 12678-12685.
45. Turzhitsky, V.; Zhang, L.; Horowitz, G. L.; Vitkin, E.; Khan, U.; Zakharov, Y.; Qiu, L.; Itzkan, I.; Perelman, L. T., Picoanalysis of Drugs in Biofluids with Quantitative Label‐Free Surface‐Enhanced Raman Spectroscopy. *Small* **2018,** *14* (47), 1802392.
46. Salemmilani, R.; Moskovits, M.; Meinhart, C. D., Microfluidic analysis of fentanyl-laced heroin samples by surface-enhanced Raman spectroscopy in a hydrophobic medium. *Analyst* **2019,** *144* (9), 3080-3087.
47. Wang, K.; Xu, B.; Wu, J.; Zhu, Y.; Guo, L.; Xie, J., Elucidating fentanyls differentiation from morphines in chemical and biological samples with surface‐enhanced Raman spectroscopy. *Electrophoresis* **2019,** *40* (16-17), 2193-2203.
48. Wang, L.; Deriu, C.; Wu, W.; Mebel, A. M.; McCord, B., Surface‐enhanced Raman spectroscopy, Raman, and density functional theoretical analyses of fentanyl and six analogs. *Journal of Raman Spectroscopy* **2019,** *50* (10), 1405-1415.
49. Lee, P.; Meisel, D., Adsorption and surface-enhanced Raman of dyes on silver and gold sols. *The Journal of Physical Chemistry* **1982,** *86* (17), 3391-3395.
50. Leonard, J.; Haddad, A.; Green, O.; Birke, R. L.; Kubic, T.; Kocak, A.; Lombardi, J. R., SERS, Raman, and DFT analyses of fentanyl and carfentanil: Toward detection of trace samples. *Journal of Raman Spectroscopy* **2017,** *48* (10), 1323-1329.
51. Rana, V.; Cañamares, M. V.; Kubic, T.; Leona, M.; Lombardi, J. R., Surface‐enhanced Raman Spectroscopy for Trace Identification of Controlled Substances: Morphine, Codeine, and Hydrocodone. *Journal of forensic sciences* **2011,** *56* (1), 200-207.
52. Tyagi, S.; Kramer, F. R., Molecular beacons: probes that fluoresce upon hybridization. *Nat. Biotechnol.* **1996,** *14* (3), 303-308.
53. Bao, C.; Conde, J.; Curtin, J.; Artzi, N.; Tian, F.; Cui, D., Bioresponsive antisense DNA gold nanobeacons as a hybrid in vivo theranostics platform for the inhibition of cancer cells and metastasis. *Scientific reports* **2015,** *5*, 12297.
54. Harry, S. R.; Hicks, D. J.; Amiri, K. I.; Wright, D. W., Hairpin DNA coated gold nanoparticles as intracellular mRNA probes for the detection of tyrosinase gene expression in melanoma cells. *Chemical Communications* **2010,** *46* (30), 5557-5559.
55. Qiao, G.; Gao, Y.; Li, N.; Yu, Z.; Zhuo, L.; Tang, B., Simultaneous Detection of Intracellular Tumor mRNA with Bi‐Color Imaging Based on a Gold

Nanoparticle/Molecular Beacon. *Chemistry–A European Journal* **2011,** *17* (40), 11210-11215.

56. Pan, W.; Yang, H.; Li, N.; Yang, L.; Tang, B., Simultaneous visualization of multiple mRNAs and matrix metalloproteinases in living cells using a fluorescence nanoprobe. *Chemistry–A European Journal* **2015,** *21* (16), 6070-6073.
57. Xue, J.; Shan, L.; Chen, H.; Li, Y.; Zhu, H.; Deng, D.; Qian, Z.; Achilefu, S.; Gu, Y., Visual detection of STAT5B gene expression in living cell using the hairpin DNA modified gold nanoparticle beacon. *Biosens. Bioelectron.* **2013,** *41*, 71-77.
58. Tsourkas, A.; Behlke, M. A.; Rose, S. D.; Bao, G., Hybridization kinetics and thermodynamics of molecular beacons. *Nucleic Acids Res.* **2003,** *31* (4), 1319-1330.
59. Frens, G., Controlled nucleation for the regulation of the particle size in monodisperse gold suspensions. *Nature physical science* **1973,** *241* (105), 20-22.
60. Song, S.; Liang, Z.; Zhang, J.; Wang, L.; Li, G.; Fan, C., Gold‐nanoparticle‐based multicolor nanobeacons for sequence‐specific DNA analysis. *Angewandte Chemie International Edition* **2009,** *48* (46), 8670-8674.
61. Liu, X.; Atwater, M.; Wang, J.; Huo, Q., Extinction coefficient of gold nanoparticles with different sizes and different capping ligands. *Colloids Surf. B. Biointerfaces* **2007,** *58* (1), 3-7.